The turquoise-chalcosiderite Cu(Al,Fe^{3+})$_6$(PO$_4$)$_4$(OH)$_8$·4H$_2$O solid-solution series: A Mössbauer spectroscopy, XRD, EMPA, and FTIR study

Yassir A. Abdu,[1,*] Sharon K. Hull,[2] Mostafa Fayek,[1] and Frank C. Hawthorne[1]

[1]Department of Geological Sciences, University of Manitoba, Winnipeg, Manitoba R3T 2N2, Canada
[2]Department of Anthropology, University of Manitoba, Winnipeg, Manitoba R3T 2N2, Canada

Abstract

Eight turquoise samples covering a wide range of compositions in the turquoise-chalcosiderite solid-solution series were analyzed by Mössbauer spectroscopy, X-ray diffraction (XRD), electron microprobe analysis (EMPA), and Fourier transform infrared (FTIR) spectroscopy. Two of the turquoise samples display evidence of alteration from weathering processes. The unit formulas were calculated on the basis of 24 (O,OH) anions and 11 cations using the results of EMPA, assuming all Fe as Fe^{3+}, as confirmed by Mössbauer spectroscopy. The altered turquoise samples show deficiencies in both cations and anion groups, indicated by EMPA, but they preserve the crystal structure of turquoise, as verified by XRD. They also show large amounts of Si and Ca in their microprobe data, due to the presence of kaolinite and Ca carbonate, respectively, which are identified by FTIR spectroscopy. The isomorphous substitution of Fe^{3+} for Al in the turquoise structure broadens and shifts the IR bands to lower frequencies, in particular the OH-stretching bands. The Mössbauer spectra, collected at room temperature, are fitted with two generalized Fe^{3+} sites, using a Voigt-based quadrupole-splitting distribution method, which are assigned to the M3 (smaller quadrupole splitting) on the one hand and M1 and M2 octahedral sites on the other hand. The Fe^{3+} distribution over the M3 and M1,2 sites, calculated from the Mössbauer relative areas and EMPA, indicates that Fe^{3+} prefers the larger M3 octahedron in the turquoise-chalcosiderite solid-solution series.

Keywords: Turquoise, chalcosiderite, alteration, Castillian Mine, Tyron Mine, Cornwall, electron microprobe analysis, FTIR, Mössbauer spectroscopy

Introduction

Turquoise is common in the American Southwest, where most of its value is associated with art (e.g., jewelry) and Native American culture. There has been renewed interest in this complex mineral due to a recently developed technique that can identify the provenance regions of turquoise artifacts using the isotopic ratios of hydrogen and copper (Hull et al. 2008). This approach allows archaeologists to reconstruct and investigate pre-Colombian turquoise trade structures, and gemologists to authenticate the source of turquoise (e.g., Lone Mountain mine in Nevada vs. Sleeping Beauty mine in Arizona).

When affected by near-surface conditions and extended exposure to sunlight and meteoric (rain) water, turquoise weathers to chalky white clay minerals. This alteration affects identification of the provenance regions of archaeologically recovered turquoise artifacts (Hull et al. 2008), the mineralogical properties of turquoise, and the value of turquoise as a semi-precious gemstone. However, this alteration process is poorly understood. Therefore, to improve the characterization of turquoise provenance for archaeological and gemological purposes, it is important to understand the alteration processes that affect turquoise.

In this work, we characterize turquoise samples covering a wide range of compositions in the turquoise-chalcosiderite series by X-ray diffraction (XRD), electron microprobe analysis

(EMPA), FTIR and Mössbauer spectroscopy, to (1) learn more about turquoise alteration and (2) study the distribution of Fe between the metal sites.

Background

Turquoise is a hydrated copper aluminum phosphate and belongs to a group of minerals, the turquoise group, consisting of at least six isostructural end-members (Table 1; Foord and Taggart 1998). The general formula for the turquoise group may be written as A$_{0-1}$B$_6$(PO$_4$)$_4$(OH)$_8$·4H$_2$O with Cu^{2+} or Fe^{2+} as the most common constituents at the A position and Al^{3+} and Fe^{3+} at the B position. However, Ca^{2+} or Zn^{2+} can occur at the A position in some of the more rare members of the turquoise group. The range in chemical composition (i.e., different concentrations of Cu, Fe, and Al) of turquoise (sensu lato) produces a wide range of colors (Table 1). Foord and Taggart (1998) suggest that differences in the Cu and Fe ratio are responsible for the differences in color of the samples: blue turquoise has Cu at the A position and Al at the B position, whereas green turquoise (chalcosiderite) largely contains Fe^{3+} at the B position.

The crystal structure of turquoise is triclinic, space group $P\bar{1}$, and is illustrated in Figure 1. Different site nomenclatures have been used in many of the structural and spectroscopic studies of the minerals of the turquoise group, depending on the chemical compositions under study. Here we use a more general site nomenclature that avoids phrases as for example "Fe^{3+} occupying an Al site". There are four sites that are octahe-

TABLE 1. Minerals of the turquoise group

Mineral	Chemical formula	Color	Luster	Hardness
Aheylite	$Fe^{2+}Al_6(PO_4)_4(OH)_8\cdot4(H_2O)$	pale blue, green and blue-green	vitreous, dull	5–5.5
Chalcosiderite	$CuFe^{3+}_6(PO_4)_4(OH)_8\cdot4(H_2O)$	apple green, darkgreen	vitreous, glassy	4.5
"Coeruleolactite"	$(Ca,Cu)Al_6(PO_4)_4(OH)_8\cdot4–5(H_2O)$	milk white, light blue	vitreous, waxy	5
Faustite	$(Zn,Cu)Al_6(PO_4)_4(OH)_8\cdot4(H_2O)$	apple green	chalky, earthy, dull	5.5
Planerite	$\square Al_6(PO_4)_2(PO_3OH)_2(OH)_8\cdot4(H_2O)$	white, olive green, pale blue, green and blue-green	vitreous, dull	5
Turquoise	$CuAl_6(PO_4)_4(OH)_8\cdot4(H_2O)$	pale green, blue-green, turquoise blue	waxy	5–6

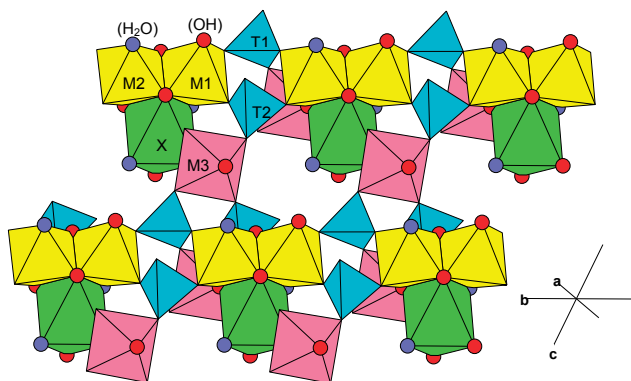*Note*: Mineral and chemical formulas from Foord and Taggart (1998).

FIGURE 1. The crystal structure of turquoise; M1 and M2 octahedra are shown in yellow, M3 octahedra are shown in pink, X octahedra are shown in green, and T tetrahedra are shown in blue; hydrogen bonds are omitted for clarity. (OH) and (H_2O) groups are shown as red and blue circles, respectively.

drally coordinated by O^{2-} and $(OH)^-$ anions and two T sites that are tetrahedrally coordinated by O^{2-} anions, and are occupied by P. The octahedrally coordinated sites may be divided into two groups, the M1–M3 sites that are occupied dominantly by small trivalent cations, and the X site that is occupied by medium-sized divalent cations (primarily Cu^{2+}, Fe^{2+}, and Zn). Thus, the structural formula for turquoise is X $(M1_2M2_2M3_2)_{\Sigma=6}$ $(PO_4)_4(OH)_8\cdot4H_2O$. In the structure of turquoise (Fig. 1), pairs of edge-sharing M1 and M2 octahedra are linked by sharing corners with pairs of T tetrahedra to form chains that extend in the **b** direction. These chains are linked in the **a** and **c** directions by sharing corners with M3 octahedra, and further linkage is provided by X octahedra that share edges with the M1 and M2 octahedra. The heteropolyhedral framework is strengthened by a network of hydrogen bonds involving the (OH) groups in the formula. Of particular importance in Figure 1 are the similarities and differences exhibited by the M1–M3 octahedra. The M1 and M2 octahedra are very similar in their general stereochemistry and their linkage to adjacent cation polyhedra is identical. On the other hand, the local stereochemistry of the M3 octahedron is very different from that of M1 and M2. It does not share any edges with the M1 and M2 octahedra and shares a corner with the X octahedron (Fig. 1). Thus similar behavior is expected from constituents occupying the M1 and M2 octahedra and different behavior from constituents occupying the M3 octahedron.

Substitution of Al by Fe^{3+} results in the solid-solution series turquoise-chalcosiderite: $Cu(Al,Fe^{3+})_6(PO_4)_4(OH)_8\cdot4H_2O$. Cid-Dresdner and Villarroel (1972) studied rashleighite, an intermediate member of the series, by powder X-ray diffraction, and concluded that Fe^{3+} is statistically distributed over the three

Al sites (i.e., M sites in our notation). However, Giuseppetti et al. (1989) refined the crystal structure of an Al-bearing chalcosiderite (Al = 0.54 apfu) and found that Fe^{3+} is partly ordered at the Fe1 site (corresponds to Al3 site in the work of Cid-Dresdner 1965). The Al1 and Al2 sites were labeled by Giuseppetti et al. (1989) as Fe2A and Fe2B, respectively. Giuseppetti et al. (1989) also reanalyzed the powder X-ray diffraction data of Cid-Dresdner and Villarroel (1972) for rashleighite and cautiously suggested similar behavior of Fe^{3+} in intermediate compositions of the series, where it is very difficult to find single crystals suitable for X-ray diffraction.

[57]Fe Mössbauer spectroscopy, due to its ability to probe the local environment of the Fe nucleus regardless of the degree of sample crystallinity, can be used to verify the Fe^{3+} site preference in the turquoise-chalcosiderite series. To our knowledge, the work done on turquoise that involves Mössbauer spectroscopy is very scarce (Belyaev and Ievlev 1989; Sklavounos et al. 1992), and the technique has never been used to address the above issue in turquoise. Other Mössbauer studies of hydrated phosphate minerals are reported by Amthauer and Rossman (1984), Da Costa et al. (2005), and De Resende et al. (2008).

Fourier-transform infrared (FTIR) spectroscopy is a valuable technique in studying hydrated minerals. It is very sensitive to the hydroxyl (OH) group and can easily distinguish between OH in the structure and H_2O molecules. The technique can be used to supplement X-ray diffraction and chemical analysis, as FTIR spectra can be easily obtained for crystalline as well as poorly crystalline materials. Recently, Reddy et al. (2006) studied in detail two Fe-bearing turquoise samples from Arizona (U.S.A.) and the Kouroudaiko mine (Senegal), with Fe_2O_3 contents of 1.94 and 3.19 wt%, respectively, by FTIR spectroscopy and assigned the different vibrational bands for both the hydroxyl (OH) and the phosphate $(PO_4)^{3-}$ groups.

MATERIALS AND EXPERIMENTAL METHODS

The provenances of the turquoise samples used in this study are given in Table 2. The samples were characterized by powder XRD using a Philips (PANalytical) PW1710 automated diffractometer with CuKα radiation. The PW1710 system consists of a 4kW sealed-tube type X-ray generator in a housing with a centrally located tube tower and vertical goniometer with Bragg-Brentano (θ–2θ) geometry. The goniometer is equipped with a graphite monochromator in the diffracted beam and a scintillation detector. The microprocessor is operated remotely from a PC using MDI DataScan software and data are processed using MDI Jade+ software.

Backscattered electron images and electron microprobe analysis were done

TABLE 2. Sample provenance

Sample(s)	Provenance
CS-1, Cas-1, Cas-4a, Cas-4c	Castillian Mine, Cerrillos Hills, New Mexico, U.S.A.
Ty-1	Tyron Mine, New Mexico, U.S.A.
GT-1	Green Tree, Nevada, U.S.A.
Ry-1	Royston, Nevada, U.S.A.
Chalcosiderite	Cornwall, England

using a CAMECA SX-100. Chemical analysis were obtained using wavelength-dispersion mode with the following conditions: excitation voltage: 15 kV; specimen current: 10 nA; beam size: 10 μm. Mean chemical compositions for all samples are given in Table 3, together with the unit formulas normalized to 24 (O, OH) anions and 11 cations. As can be seen from Table 3, the chemical compositions of the turquoise samples cover a wide range of the turquoise-chalcosiderite series. The Al-bearing chalcosiderite used in this study is from the same locality as that studied by Giuseppetti et al. (1989), Cornwall, England, and its Fe and Al contents obtained by microprobe analysis (Table 3) are similar to those determined by X-ray crystal-structure refinement (Giuseppetti et al. 1989).

FTIR spectra were collected using a Bruker Tensor 27 FTIR spectrometer equipped with a KBr beam splitter and a DLATGS detector. Spectra over the range 4000–400 cm^{-1} were obtained by averaging 100 scans with a resolution of 4 cm^{-1}. Powdered samples were prepared as KBr pellets, with a sample/KBr ratio of ~1%. Base-line correction was done using the OPUS spectroscopic software (Bruker Optic GmbH).

Mössbauer spectroscopy measurements were done at room temperature (RT) using a ^{57}Co(Rh) point source. Mössbauer absorbers were prepared by mixing the sample with powdered sugar and loading the mixture into a sample holder containing ~5 mg Fe/cm^2. The spectrometer was calibrated with the RT spectrum of α-Fe in the velocity range of ±4 mm/s. The spectra were analyzed by a Voigt-based quadrupole-splitting-distribution (QSD) method (Rancourt and Ping 1991) implemented in the Recoil software. To account for absorber-thickness and instrumental broadening, the Lorentzian linewidth of the elemental doublets of the QSD was allowed to vary during the spectrum fitting procedure (Rancourt 1994).

RESULTS AND DISCUSSION

Alteration

Three samples were collected from the Castillian Mine pit (Cas-1, Cas-4a, Cas-4c) and one sample (CS-1) was provided by Douglas Magnus, owner of the Castillian turquoise mine, New Mexico. These samples showed variable alteration. On visual inspection, the variation of hardness and colors of the samples

collected within the mine pit supports the assumption that the most exposed samples were the most altered, because these were much lighter in color and could be easily crumbled with the slightest pressure (Figs. 2a and 2b). The samples were collected from fractures and veinlets where turquoise occurs along the wall of the 25 m deep mine pit. The least-altered Castillian sample, Cas-1, was collected from the bottom of the pit, Cas-4a (altered) was collected approximately 13 m below the ground surface, and Cas-4c (altered) was collected from a vein that ran vertically through the mine pit located near Cas-4a. SEM images of the surface of the unaltered turquoise sample (Cas-1) show a blocky, crystalline texture (Fig. 3a), whereas altered turquoise (Cas-4a) has a platy surface (Fig. 3b).
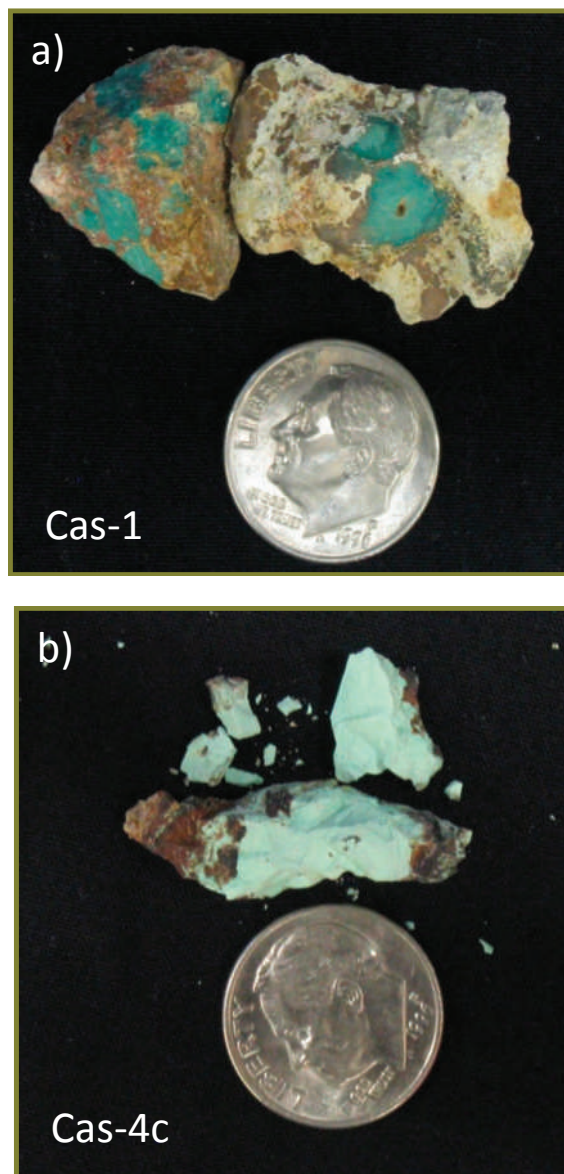
FIGURE 2. Images of turquoise hand specimens. (**a**) Dark green, least altered Castillian sample, Cas-1, collected from the bottom of the Castillian mine pit; (**b**) Cas-4c (altered) was collected from a vein that ran vertically through the mine pit. Note the lighter green color and crumbling nature of the altered turquoise.
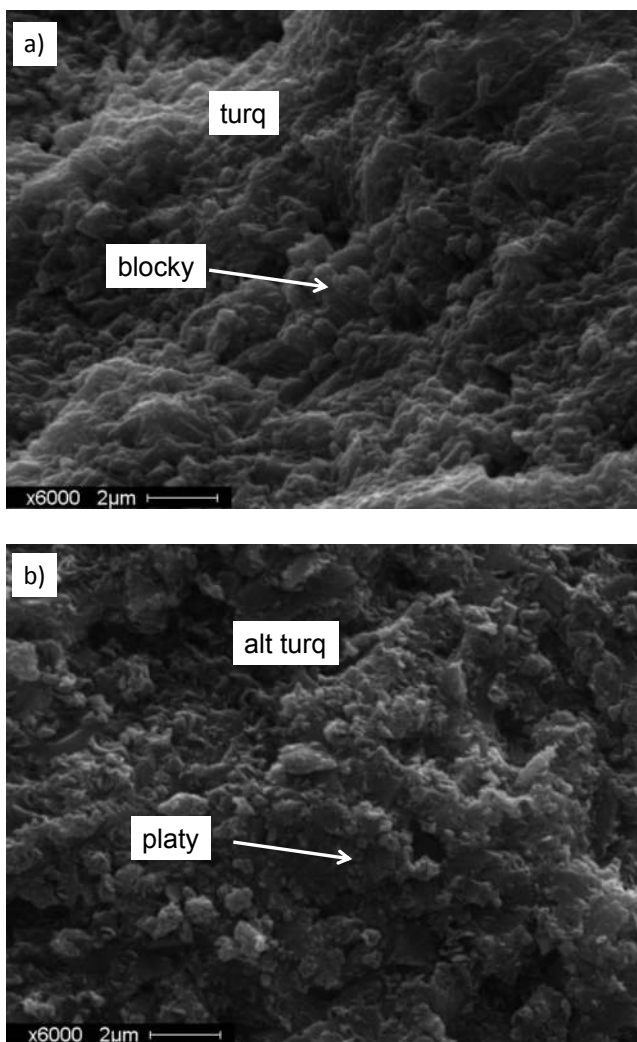
TABLE 3. Average chemical composition (wt%) and unit formula (apfu), based on 24 (O,OH) and 11 cations, for turquoise

	GT-1	Ry-1	Ty-1	CS-1	Cas-4a	Cas-4c	Cas-1	Chalco-siderite
no.*	10	5	9	10	10	10	10	10
P_2O_5	34.43	35.58	31.45	32.78	21.96	26.24	31.07	28.50
SiO_2	0.02	0.38	1.07	0.03	18.13	5.82	0.02	0.06
SO_3	0.17	0.14	0.21	0.56	0.40	4.56	1.21	n.a.
Al_2O_3	35.68	35.71	26.45	26.73	14.45	20.46	18.04	2.56
Fe_2O_3	2.07	2.50	14.38	14.53	16.87	16.45	25.49	44.07
Cr_2O_3	0.20	n.a.	0.02	0.02	0.02	0.01	0.02	0.02
CuO	8.96	8.82	8.96	7.68	5.99	6.66	7.23	8.11
ZnO	0.18	n.a.	0.04	0.08	0.07	0.07	0.01	0.08
TiO_2	0.02	n.a.	0.01	n.d.	n.d.	n.d.	0.09	n.d.
MgO	0.01	n.a.	0.02	0.01	0.44	0.21	n.d.	n.d.
CaO	0.22	0.07	0.07	0.12	8.89	3.70	0.01	0.03
K_2O	0.06	n.a.	0.08	0.11	0.11	0.07	0.08	0.05
H_2O†	18.00	16.84	17.27	17.46	12.74	16.64	16.96	16.49
Total	100.02	100.04	100.03	100.11	100.07	100.89	100.23	99.97
P	3.99(3)	4.08(2)	3.81(4)	3.97(6)	2.50(39)	3.16(11)	3.95(4)	3.98(5)
Si	0.00	0.05	0.15(2)	0.00	2.4(8)	0.83(18)	0.00	0.01
S	0.02	0.01	0.02	0.06	0.04	0.49(19)	0.14(1)	n.a.
Al	5.76(3)	5.69(3)	4.46(5)	4.51(14)	2.29(40)	3.43(20)	3.19(14)	0.50(11)
Fe	0.21(1)	0.25(1)	1.55(2)	1.57(11)	1.71(26)	1.76(10)	2.88(15)	5.47(6)
Cr	0.02	n.a.	0.00	0.00	0.00	0.00	0.00	0.00
Ti	0.00	n.a.	0.00	n.d.	n.d.	n.d.	0.01	n.d.
Cu	0.93(1)	0.90(1)	0.97(2)	0.83(3)	0.61(9)	0.71(5)	0.82(3)	1.01(2)
Zn	0.02	n.a.	0.00	0.01	0.01	0.01	0.00	0.01
Mg	0.00	n.a.	0.00	0.00	0.09(3)	0.04	n.d.	n.d.
Ca	0.03	0.01	0.01	0.02	1.3(12)	0.56(25)	0.00	0.01
K	0.01	n.a.	0.01	0.02	0.02	0.01	0.02	0.01
OH‡	16.4(3)	15.2(2)	16.5(5)	16.7(6)	11.4(3)	15.8(5)	17.0(5)	18.1(3)

Notes: n.a. = not analyzed, n.d. = not detected.
* Number of spots.
† Calculated by difference.
‡ OH + H$_2$O.

FIGURE 3. SEM images of (**a**) unaltered turquoise (sample Cas-1) with a crystalline blocky morphology, and (**b**) altered turquoise (Cas-4a) with a platy surface.
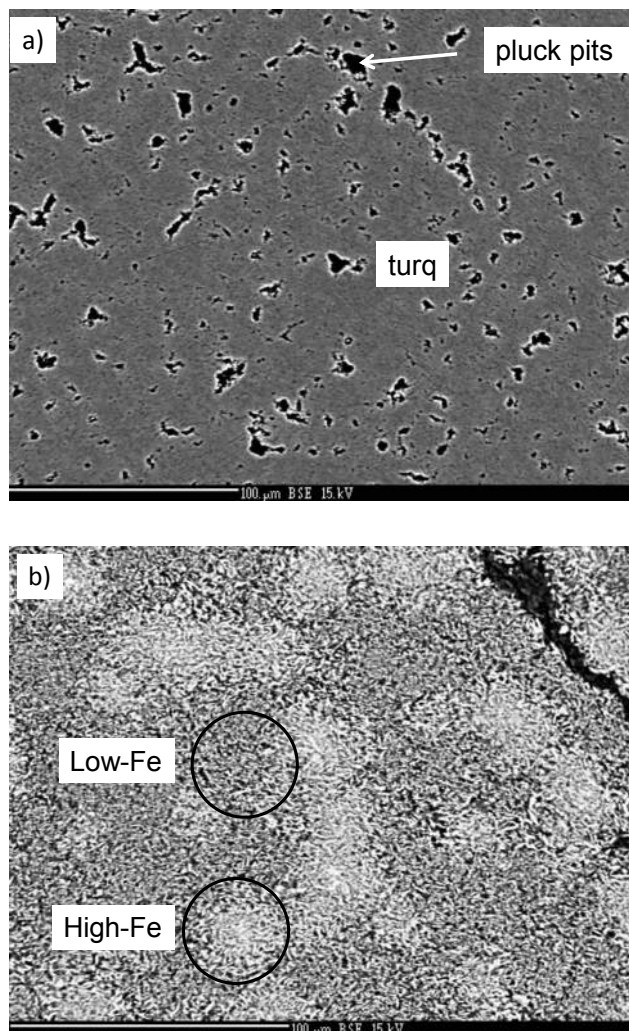

FIGURE 4. Backscattered electron images of (**a**) Cas-1, unaltered turquoise, showing a relatively homogenous reflectance and pluck pits due to polishing, and (**b**) Cas-4a, altered turquoise, with a much more porous and fibrous surface consisting of patches with low and high Fe.

Detailed petrography of the altered and unaltered samples shows distinct textural differences (Fig. 4). Backscattered electron images (BSE) of unaltered turquoise (Cas-1) show a relatively homogenous texture with a few pluck marks due to polishing, which appear as voids (Fig. 4a). Altered turquoise (Cas-4a) shows a highly porous and fibrous texture with rosettes that are higher in Fe contents than the matrix (Fig. 4b). However, altered turquoise generally has lower Fe content relative to unaltered turquoise (Fig. 5a).

Figure 5a shows the variation of Al_2O_3 as a function of Fe_2O_3 for all samples using the microprobe data of all analyzed spots. Data for the majority of the turquoise samples lie along the ideal line (dashed line in Fig. 5a) connecting the end-member compositions of the turquoise-chalcosiderite series, ideal turquoise (Al_2O_3 = 37.60 wt%) and ideal chalcosiderite (Fe_2O_3 = 48.55 wt%). However, the data points of the altered turquoise samples (Cas-4a and Cas-4c) deviate significantly from this line (Fig. 5a) because the B site in the altered samples has variable cation deficiency, i.e., Al + Fe <6 apfu (Fig. 5b, Table 3). The altered samples show

a negative correlation between P_2O_5 and (SiO_2+SO_3) (Fig. 6), which may indicate that P is leached from the turquoise structure and replaced by Si and/or S during the alteration process. The samples also contain Ca, the abundance of which correlates with the Cu deficiency (Table 3). It is unlikely that Ca replaces Cu at the A site, and the existence of a Ca-dominant A site member of the turquoise group "coeruleolactite" is doubted by Foord and Taggart (1998). They further suggested that the A-site deficiency in turquoise, which is accompanied by an excess of H_2O, can be accounted for by protonation of the $(PO_4)^{3-}$ groups to form plane-rite [$\square Al_6(PO_4)_2(PO_3OH)_2(OH)_8 \cdot 4(H_2O)$]. The A-site deficiency in the altered samples is accompanied by lower H_2O contents, as well as deficiencies at the B and P sites (Table 3), but the crystal structure of turquoise is maintained, as verified by XRD (Fig. 7). This is in agreement with the work of Van Wambeke (1971) on the alteration of some phosphates, where the alteration process can sometimes cause cation and anion deficiencies, with preservation of the structure. Thus, the presence of Si and Ca in
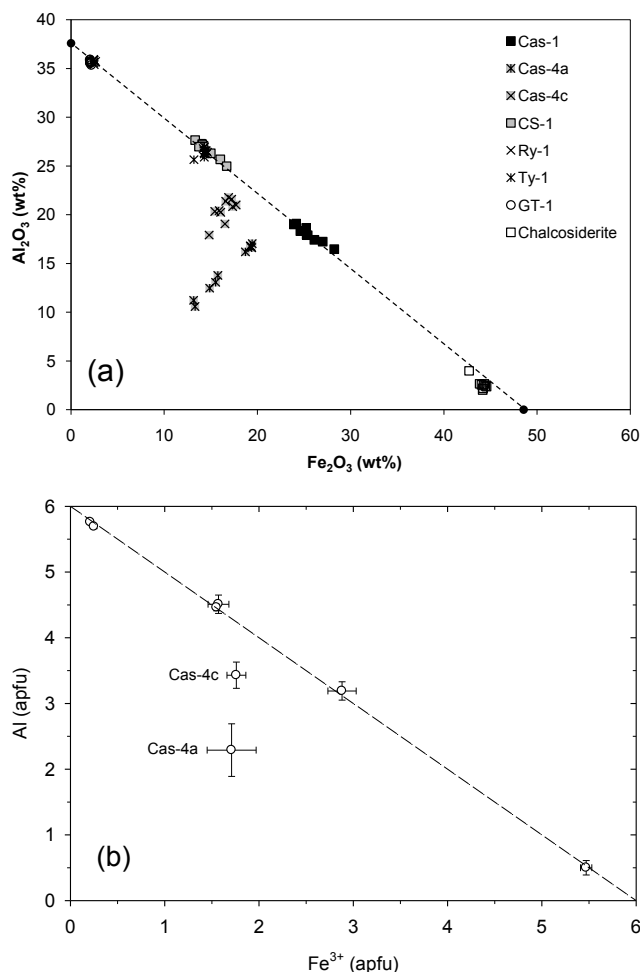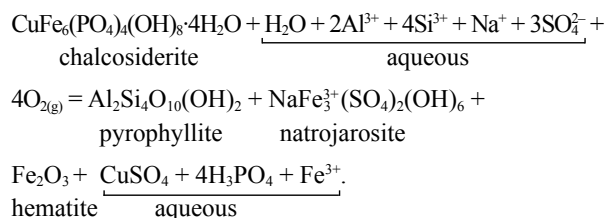
FIGURE 5. (**a**) Al_2O_3 vs. Fe_2O_3 of all microprobe data for turquoises; (**b**) average Al vs. Fe^{3+} (apfu) for turquoises plotted from the data in Table 3. Error bars are smaller than the symbol when not visible. The dashed line connects ideal-turquoise to ideal-chalcosdierite.

the altered samples, as indicated by EMPA (Table 3), could be due to impurity phase(s) that escaped detection by XRD, due to its very low concentration or poor crystallinity.

Based on EMPA and detailed petrography, the alteration of turquoise could be the result of the following reaction

$$CuFe_6(PO_4)_4(OH)_8·4H_2O + \underline{H_2O + 2Al^{3+} + 4Si^{3+} + Na^+ + 3SO_4^{2-} +}$$

chalcosiderite   aqueous

$$4O_{2(g)} = Al_2Si_4O_{10}(OH)_2 + NaFe_3^{3+}(SO_4)_2(OH)_6 +$$

pyrophyllite   natrojarosite

$$Fe_2O_3 + \underline{CuSO_4 + 4H_3PO_4 + Fe^{3+}}.$$

hematite   aqueous

FTIR

Figure 8 shows the FTIR spectra in the range 4000–400 cm^{-1} for all samples. The bands in the region 4000–2500 cm^{-1} are due to OH-stretching vibrations of the OH groups and H_2O molecules in the turquoise structure. The broad band at 1600 cm^{-1} is associated with the H-O-H bending vibrations of the H_2O
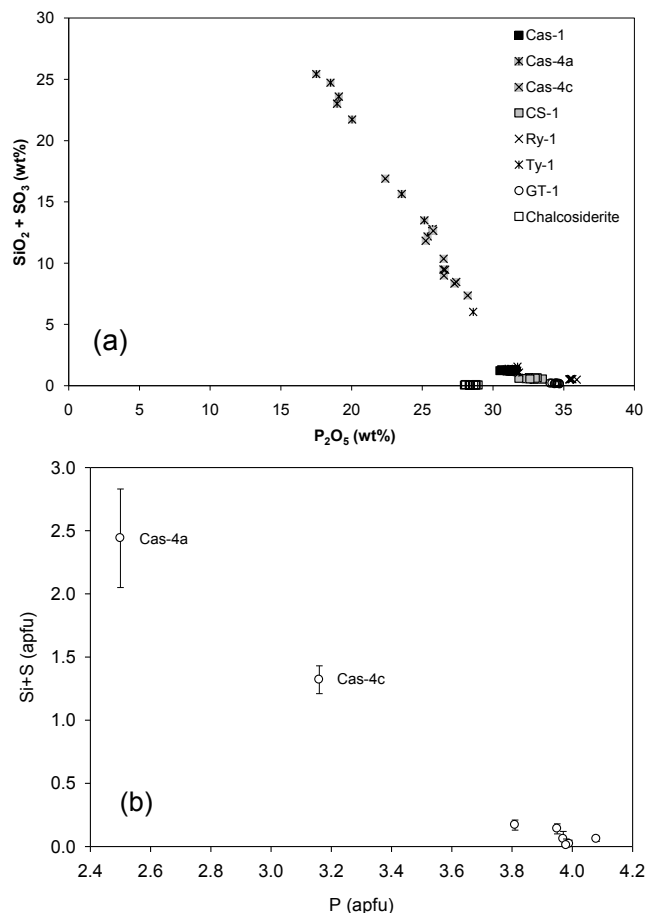

FIGURE 6. (**a**) (SiO_2+SO_3) vs. P_2O_5 of all microprobe data for turquoises; (**b**) average $(Si+S)$ vs. P (apfu) for turquoises plotted using the data in Table 3. Error bars are smaller than the symbol when not visible.

molecules. The P-O stretching vibrations of the phosphate group $(PO_4)^{3-}$ are located between 1200–900 cm^{-1} and the bands in the region below 900 cm^{-1} are mainly due to coupled motions of the frameworks of tetrahedra and octahedra

The unit cell of turquoise contains four OH groups and two H_2O molecules. Thus, an FTIR spectrum of turquoise in the OH region is expected to show four sharp OH-stretching bands from the OH groups and two broad bands from the H_2O molecules. The FTIR spectra of the GT-1 and Ry-1 samples are very similar, and show five bands in the OH-stretching region. For GT-1, three sharp OH-stretching bands occur at 3510, 3467, and 3451 cm^{-1}, and two broad bands of the H_2O molecules are found at 3287 and 3070 cm^{-1} (Fig. 8), very similar to the bands reported for Arizona turquoise by Reddy et al. (2006). With increasing Fe content, the OH-stretching bands become broader, the spectra gradually lose resolution, and the bands shift to slightly lower frequencies, which is most evident in the spectrum of chalcosiderite (Fig. 8). The FTIR spectra of Cas-4a, Cas-4c, and Ty-1 samples show two extra OH-stretching bands at ~3698 and 3622 cm^{-1}, which are more pronounced in the spectrum of Cas-4c (Fig. 8). Figure 9 shows an expanded view of the region 3720–3600 cm^{-1} for the Cas-4c spectrum, where very weak bands at 3675, 3668, 3655, and 3648 cm^{-1} can be observed between the 3698 and
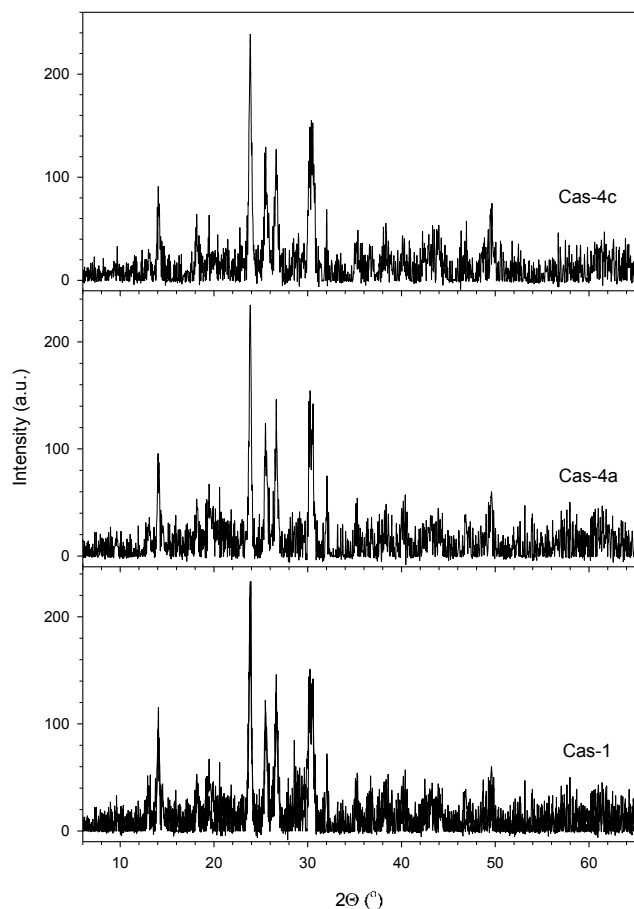
FIGURE 7. Powder X-ray diffrcation patterns of the unaltered turquoise (Cas-1) and the altered turquoises (Cas-4a and Cas-4c). All diffraction lines belong to the turquoise structure.

3622 cm^{-1} bands. These OH-stretching bands are characteristic of kaolinite-group minerals (Prost et al. 1989; Johansson et al. 1998; Madejová and Komadel 2001). The Si-O stretching bands of kaolinite, which occur at ~1000–1100 cm^{-1}, are not resolved due to the strong overlap with the P-O stretching bands of the $(PO_4)^{3-}$ group in turquoise. However, the Si-O-Si bending band at ~470 cm^{-1}, as well as the OH-bending of the inner OH groups at ~912 cm^{-1} (Madejová and Komadel 2001), can easily be identified in the FTIR spectra of Cas-4c and Cas-4a samples (Fig. 10).

The FTIR spectra of the Cas-4a and Cas-4c samples (Fig. 8) also show weak bands centered at 1430 and 1460 cm^{-1}, characteristic of the C-O stretching vibrations of the carbonate group $(CO_3)^{2-}$ (Adler and Kerr 1963). The high Ca content indicated by the electron microprobe data suggests that it is a Ca-rich carbonate. Therefore, the high Si and Ca contents of the altered turquoise samples are attributed to the presence of kaolinite and Ca carbonate, respectively, admixed with turquoise.

In the study of Reddy et al. (2006), the FTIR spectrum of the turquoise from Arizona (Fe$_2$O$_3$ = 1.94 wt%) showed three OH-stretching bands, similar to those observed in the FTIR spectrum of the GT-1 sample (Fe$_2$O$_3$ = 2.07 wt%). However, the turquoise from Senegal (Fe$_2$O$_3$ = 3.19 wt%) shows an additional narrow OH-stretching band at 3608 cm^{-1}, which was assigned to the OH-Fe^{3+} vibrations in the turquoise structure (Reddy et al. 2006).
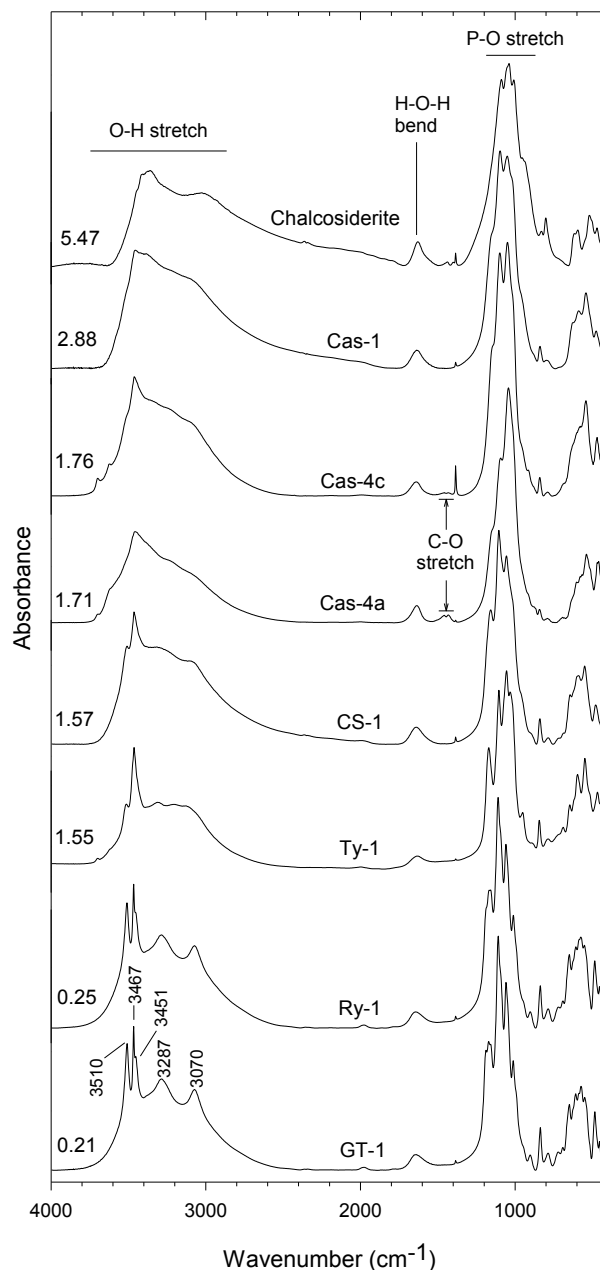

FIGURE 8. FTIR spectra for turquoises. The numbers on the left side are the total Fe content in apfu. The small sharp peak at ~1385 cm^{-1} is an artifact from the KBr pellet.

No such band was observed in the FTIR spectra of our turquoise samples, which have variable amounts of Fe^{3+}. Therefore, the 3608 cm^{-1} band in the FTIR spectrum of the Senegal turquoise is most likely due to an impurity phase.

Site preference of Fe^{3+}

Mössbauer spectra. Selected room-temperature Mössbauer spectra of turquoise samples are shown in Figure 11. They generally consist of a broad Fe^{3+} doublet centered at ~0.1 and 0.7 mm/s, and a visible shoulder on the low-velocity peak, indicating the presence of at least two Fe^{3+} sites. Fe^{2+}, with its high-velocity peak located between 2 and 3 mm/s, was not detected
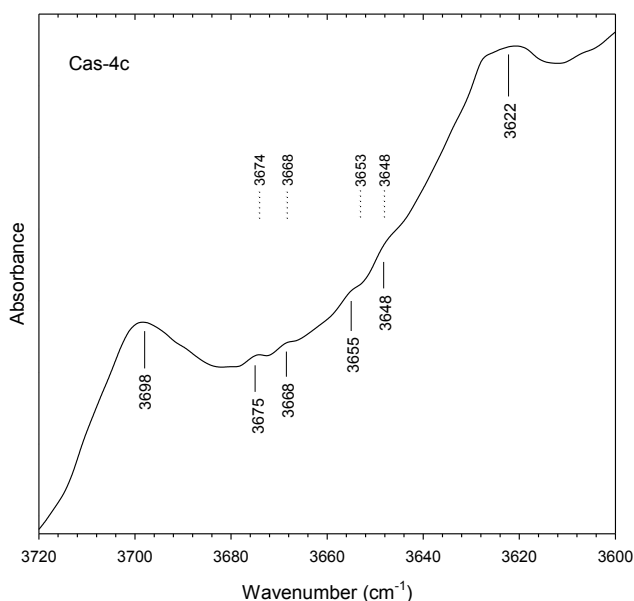
FIGURE 9. FTIR spectrum of the Cas-4c sample in the region 3720–3600 cm^{-1} showing the kaolinite OH-stretching bands. For comparison, the position of the inner bands of the OH-stretching vibrations of kaolinite reported by Johansson et al. (1998), Figure 1, are shown (dotted lines).

in any of the spectra. Consequently, the spectra were fit using a Voigt-based quadrupole-splitting distribution (QSD) to a model having two Fe^{3+} sites (each with a single Gaussian component). The hyperfine parameters for all samples are given in Table 4. The site with the smaller average quadrupole splitting (QS) is assigned to Fe^{3+} at M3 and that with the larger QS to Fe^{3+} at the M1 and M2 sites (=M1,2) based on previous work (Sklavounos et al. 1992) and the following discussion. Sklavounos et al. (1992) studied a turquoise sample with an Fe content of 0.13 apfu and fitted its Mössbauer spectrum with two Lorentzian doublets. They tentatively assigned the outer doublet (QS = 1.09 mm/s) to Fe^{3+} at the Al3 site (M3) and the inner doublet (QS = 0.52 mm/s) to Fe^{3+} at both Al1 and Al2 sites (M1 and M2), and concluded that more spectra of turquoises having different Fe contents are needed to make more reliable site assignment for Fe^{3+}.

The center shift (CS), ~0.41 mm/s for Fe^{3+} (M3) and ~0.37 mm/s for Fe^{3+} (M1,2) is characteristic of Fe^{3+} in octahedral coordination (Table 4). The QS for Fe^{3+} arises only from the lattice contribution, as the 3d^5 electronic-charge distribution is spherically symmetric and hence has a zero contribution to the

electric-field gradient. In general, the QS for Fe^{3+} is expected to increase with increasing distortion of the surrounding coordination polyhedron. The large difference between the quadrupole splittings of Fe^{3+} (M3) and Fe^{3+} (M1,2) suggests that these polyhedra differ in distortion (Table 4). The distortion parameters for the M1, M2, and M3 octahedra, calculated for turquoise (Cid-Dresdner 1965) and chalcosiderite (Giuseppetti et al. 1989) are listed in Table 5. Evidently, the M1 and M2 octahedra are more distorted and have similar distortion parameters, while the M3 octahedron is less distorted. Thus, the smaller QS of Fe^{3+} (M3) compared to that of Fe^{3+} (M1,2) can be correlated with the smaller distortion of the M3 octahedron relative to M1 and M2 octahedra. This is in accord with the positive correlation between QS and polyhedral distortion generally observed in Fe^{3+} spectra (Patrier et al. 1991). The spectral contributions of Fe^{3+} at the individual M1 and M2 sites, which are geometrically very similar, are strongly overlapping and cannot be resolved.

The Fe^{3+} site assignment made above can be verified using single-crystal structure refinement (SREF). However, with the exception of the Cornwall chalcosiderite, which was studied
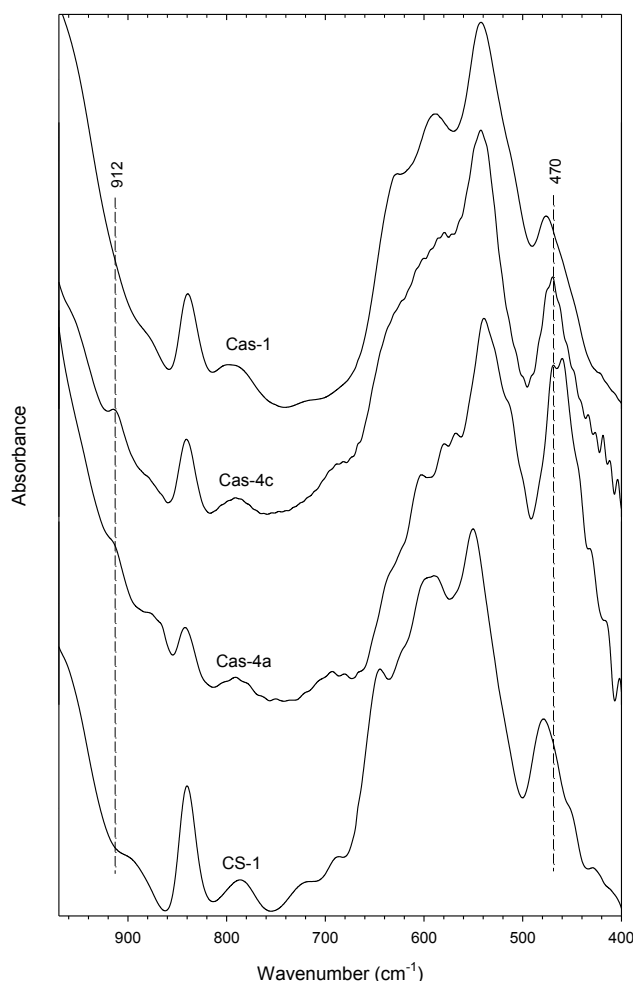

FIGURE 10. FTIR spectra of the Castillian turquoises in the region below 1000 cm^{-1}. The vertical dahsed lines mark the positions of the Si-O-Si bending (470 cm^{-1}) and OH bending of the inner OH groups (912 cm^{-1}) in kaolinite.

TABLE 4. Room-temperature Mössbauer parameters for turquoise samples

Sample	Fe^{3+} (M3)			Fe^{3+} (M1,2)		
	CS (mm/s)	QS (mm/s)	A (%)	CS (mm/s)	QS (mm/s)	A (%)
GT-1	0.406(8)	0.61(9)	65(19)	0.38(2)	1.0(1)	35(19)
Ry-1	0.41(1)	0.54(5)	69(18)	0.37(2)	1.1(3)	31(18)
Ty-1	0.411(4)	0.55(2)	81(5)	0.38(2)	1.14(8)	19(5)
CS-1	0.407(4)	0.54(2)	53(4)	0.372(5)	1.05(4)	47(4)
Cas-4a	0.399(3)	0.53(2)	60(3)	0.370(5)	1.12(3)	40(3)
Cas-4c	0.407(4)	0.53(2)	54(3)	0.370(4)	1.14(2)	46(3)
Cas-1	0.409(6)	0.57(4)	53(5)	0.379(6)	1.10(4)	47(5)
Chalcosiderite	0.419(5)	0.48(2)	37(2)	0.381(3)	1.10(1)	63(2)

Notes: CS = Center shift relative to α-Fe at RT, QS = quadrupole splitting, A = Mössbauer relative area. Standard deviations for the Mössbauer parameters were calculated using the covariance matrix of the fit.
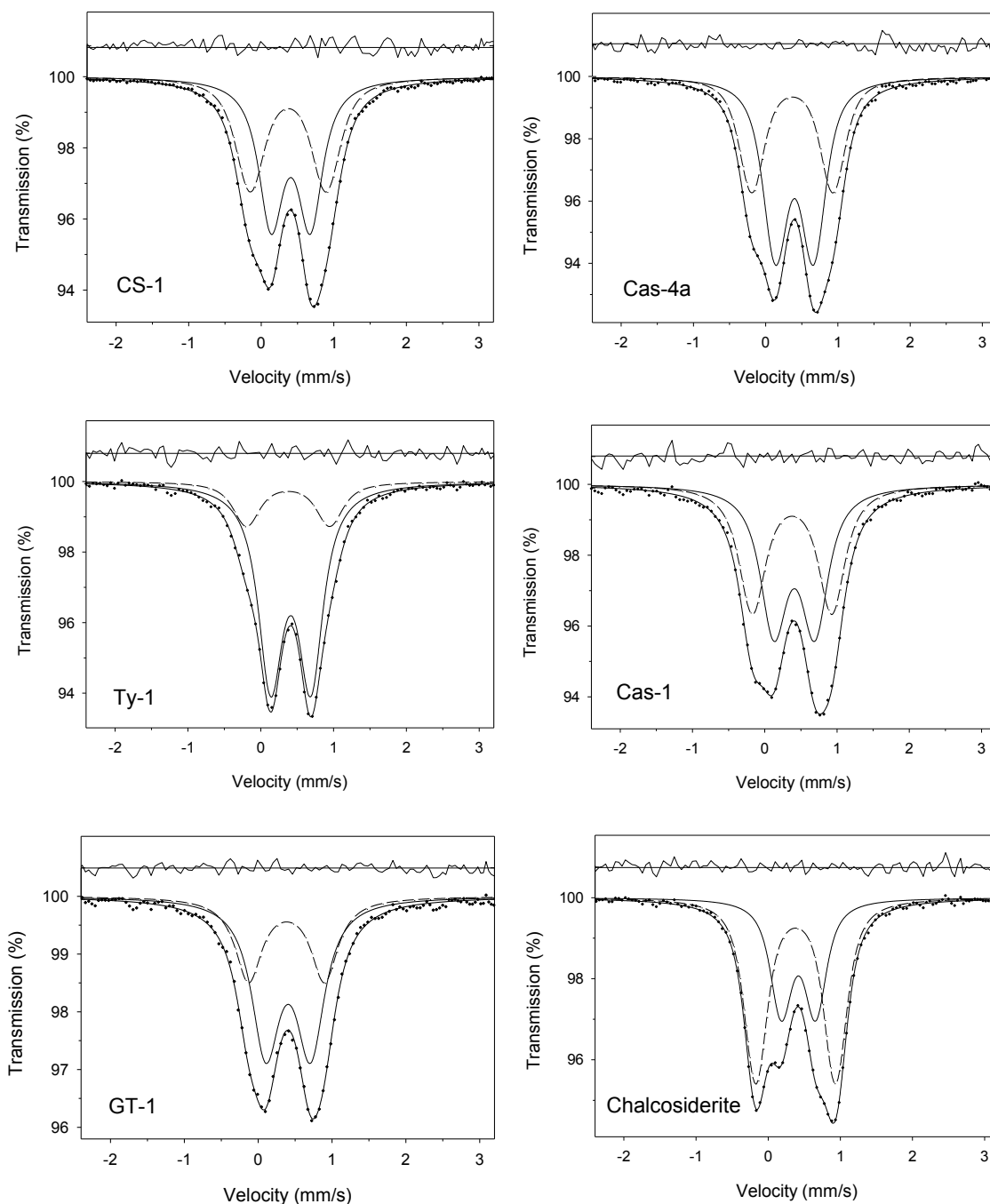
FIGURE 11. Selected room-temperature Mössbauer spectra for turquoises. Solid-line subspectra: Fe^{3+} (M3), dashed-line subspectra: Fe^{3+} (M1,2). Residuals are shown above each spectrum.

by Giuseppetti et al. (1989), the other turquoise samples do not contain single crystals suitable for SREF. The SREF data on chalcosiderite (Giuseppetti et al. 1989), which to our best knowledge is the only available SREF data on an Fe-containing turquoise, indicate that the Fe^{3+} occupancies at the M1, M2, and M3 sites are 0.88, 0.88, and 0.97, respectively. This means that 36% of Fe^{3+} is located at the M3 site and 64% at the two other sites (M1 and M2), in excellent agreement with our Mössbauer data for chalcosiderite (Table 4).

Figure 12 shows the variation of the QS as a function of composition [expressed as Fe/(Fe+Al)] for all samples. It seems

TABLE 5. Distortion parameters of the M-octahedra in turquoise and chalcosiderite calculated from the structural data of Cid-Dresdner (1965) and Giuseppetti et al. (1989), respectively

Sample	Site	λ	σ^2	Δ	V
Turquoise	M1	1.0145	42.21	0.0016	8.98
	M2	1.0161	42.93	0.0025	9.03
	M3	1.0022	4.70	0.0006	9.38
Chalcosiderite	M1	1.0172	53.47	0.0013	10.44
	M2	1.0161	46.69	0.0020	10.49
	M3	1.0023	4.98	0.0006	10.85

Note: λ and σ^2 are the mean octahedral quadratic elongation and octahedral angle variance, respectively (Robinson et al. 1971); Δ is the bond-length distortion (Fleet 1976); V is the octahedral volume. Estimated errors are better than 0.0005 for λ and Δ and better than 0.05 for σ^2 and V.

from the figure that the substitution of Fe^{3+} for Al at the M sites in the turquoise-chalcosiderite series has no significant effect on the QS of Fe^{3+}. This may indicate that the distortions of the M-octahedra have not been changed significantly by the substitution, in agreement with the crystal-structure data (Table 5).

The CS of Fe^{3+} (M3) is significantly larger than the CS for Fe^{3+} (M1,2), Table 4. Sklavounos et al. (1992) attributed this to the larger volume of the M3 octahedron compared to the M1 and M2 octahedra. A larger volume would result in a decrease in the s-electron density at the Fe nucleus and hence an increase in the CS. However, the relative increase in volume between the M1 (or M2) and M3 octahedra is just ~5% (Table 5). The octahedral volume increase as a result of the substitution of Fe^{3+} (ionic radius ≈ 0.65 Å) for Al (ionic radius ≈ 0.54 Å) from turquoise to chalcosiderite is ~16% (Table 5) and yet the CS of Fe^{3+} at the M sites does not show significant variation with composition (Table 4). Therefore, the difference in the CS between Fe^{3+} (M3) and Fe^{3+} (M1,2) cannot be due to the difference in volume between the M3 and M1,2 octahedra. The Fe^{3+} is bonded to two O, three OH, and one H_2O at the M1 and M2 sites, and four O and two OH at the M3 site (Fig. 1). Molecular orbital calculations have shown that, when OH groups replace some of the O ligands in the Fe^{3+} octahedral coordination environment, the covalent interaction between Fe^{3+} and the remaining O ligands is enhanced (Sherman 1985). Because the CS is negatively correlated with the degree of covalency for ^{57}Fe, the smaller CS for Fe^{3+} (M1,2) could be due to a relatively larger degree of covalency of the Fe-O bonds in the M1 and M2 octahedra.

Fe^{3+} distribution over the M1–M3 sites. Assuming equal recoilless fractions for Fe^{3+} (M3) and Fe^{3+} (M1,2), the Mössbauer relative areas (Table 4) represent the Fe^{3+} (M3)/Fe_{tot} and Fe^{3+} (M1,2)/Fe_{tot} ratios. As stated above, the Fe^{3+} (M1) and Fe^{3+} (M2) spectral contributions are not resolvable in our room temperature Mössbauer spectra. However, the Fe^{3+} occupancies at the M1, M2, and M3 sites in the Al-bearing chalcosiderite, determined by structure refinement, are 0.88, 0.88, and 0.97, respectively, indicating equal distribution of Fe^{3+} between the M1 and M2 sites (Giuseppetti et al. 1989). Assuming similar behavior for the distribution of Fe^{3+} between the M1 and M2 sites in the other turquoise samples, we can study the Fe^{3+}-Al order-disorder

between the M3 and M1,2 sites. The Fe^{3+} site occupancies at M3 [$X_{Fe(M3)}$] and M1,2 [$X_{Fe(M1,2)}$] are calculated by multiplying the Fe^{3+} (M3)/Fe_{tot} and Fe^{3+} (M1,2)/Fe_{tot} ratios by the total Fe obtained by microprobe analysis and dividing by the site(s) multiplicity. These occupancies can be related to a distribution parameter, K_D, defined by

$$K_D = X_{Fe(M1,2)} [1 - X_{Fe(M3)}]/X_{Fe(M3)} [1 - X_{Fe(M1,2)}],$$

where, $K_D < 1$ indicates preference of Fe^{3+} for the M3 site, $K_D > 1$ corresponds to ordering of Fe^{3+} at the M1,2 sites, and $K_D = 1$ indicates complete disorder.

Fe^{3+} site occupancies, $X_{Fe(M3)}$ and $X_{Fe(M1,2)}$, together with the K_D values, are listed in Table 6. The distribution of Fe^{3+} between the M3 and M1,2 sites is shown in Figure 13. The solid line in the figure represents complete disorder (i.e., $K_D = 1$), and the dashed curve is the calculated distribution using $K_D = 0.24$ (average value, excluding Ty-1 and chalcosiderite). For comparison, we show on the same plot the data for chalcosiderite obtained from structure refinement (Giuseppetti et al. 1989), which agrees with the Mössbauer data. Figure 13 clearly indicates that Fe^{3+} cations have preference for the M3 site in the turquoise-chalcosiderite solid-solution series. Patrier et al. (1991) observed similar behavior of Fe^{3+} in epidote, where Fe^{3+} orders at the larger octahedron, M3, while the smaller M1 and

TABLE 6. Calculated Fe^{3+} site occupancies for turquoise samples

Sample	Fe_{tot} (apfu)	$X_{Fe(M3)}$	$X_{Fe(M1,2)}$	K_D
GT-1	0.21(1)	0.07(2)	0.02(1)	0.27(16)
Ry-1	0.25(1)	0.09(2)	0.02(1)	0.21(11)
Ty-1	1.55(2)	0.63(4)	0.07(2)	0.04(1)
CS-1	1.57(11)	0.42(5)	0.18(2)	0.30(6)
Cas-4a	1.71(26)	0.51(8)	0.17(3)	0.20(6)
Cas-4c	1.76(10)	0.48(4)	0.20(2)	0.27(4)
Cas-1	2.88(15)	0.76(8)	0.34(4)	0.16(6)
Chalcosiderite	5.47(6)	1.00(6)	0.86(3)	0

Note: $K_D = X_{Fe(M1,2)} [1 - X_{Fe(M3)}]/X_{Fe(M3)} [1 - X_{Fe(M1,2)}]$.

FIGURE 13. Fe^{3+} distribution over the M3 and M1,2 sites. Solid line: complete disorder, i.e., $K_D = 1$; dashed curve: calculated distribution using $K_D = 0.24$; open circle: data from Giuseppetti et al. (1989) obtained by structure refinement. Error bars are smaller than the symbol when not visible.

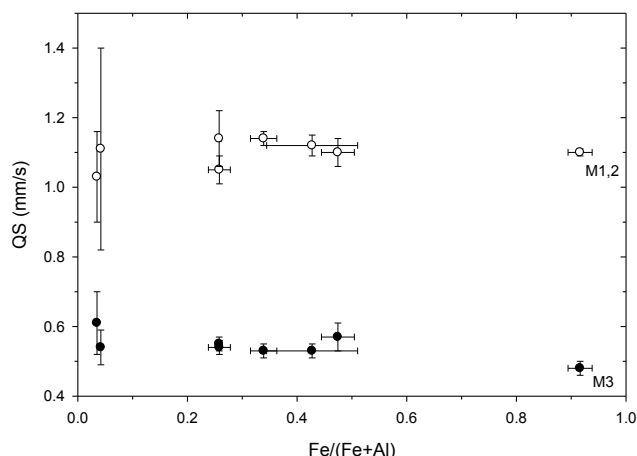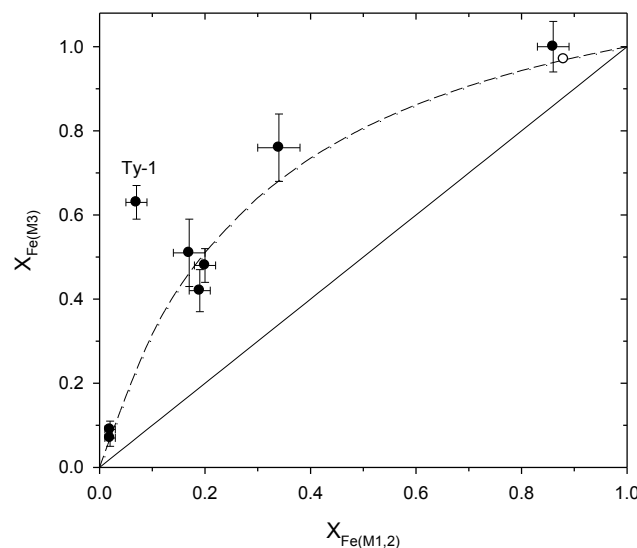**FIGURE 12.** Variation of QS with Fe/(Fe+Al) for Fe^{3+} (M3) and Fe^{3+} (M1,2). Error bars are smaller than the symbol when not visible.

M2 octahedra are predominately occupied by Al.

The turquoise sample from the Tyron Mine, Ty-1, shows strong order of Fe^{3+} at the M3 site compared to turquoises from the Castillian Mine, Figure 13, which is not obvious, given that Ty-1 and CS-1 samples have similar Fe content (Table 3). This difference in Fe^{3+} ordering may be related to the *P-T* conditions under which turquoises form, which are currently not well established.

REFERENCES CITED

Adler, H.H. and Kerr, P.F. (1963) Infrared absorption frequency trends for anhydrous normal carbonates. American Mineralogist, 48, 124–137.

Amthauer, G. and Rossman, G.R. (1984) Mixed valence of iron in minerals with cation clusters. Physics and Chemistry of Minerals, 11, 37–51.

Belyaev, A.A. and Ievlev, A.A. (1989) Arctic turquoise of Pai-Khoy (USSR). Polar Research, 7, 149–151.

Cid-Dresdner, H. (1965) Determination and refinement of the crystal structure of turquoise, $CuAl_6(PO4)_4(OH)_8.4H_2O$. Zeitschrift für Kristallographie, 121, 87–113.

Cid-Dresdner, H. and Villarroel, H.S. (1972) Crystallographic study of rashleighite, a member of the turquoise group. American Mineralogist, 57, 1681–1691.

Da Costa, G.M., Karfunkel, R.S.J, Bermanec, V., and de Sá Carneiro Chaves, M.L. (2005) ^{57}Fe-Mössbauer spectroscopy on natural eosphorite-childrenite-ernstite samples. Physics and Chemistry of Minerals, 31, 714–720.

De Resende, V.G., Da Costa, G.M., De Grave, E., and Van Alboom, A. (2008) Mössbauer spectroscopic study of synthetic leucophosphite, $KFe_2(PO_4)_2(OH)\cdot2H_2O$. American Mineralogist, 93, 483–487.

Fleet, M.E. (1976) Distortion parameters for coordination polyhedra. Mineralogical Magazine, 40, 531–533.

Foord, E.E. and Taggart, J.E. Jr. (1998) A reexamination of the turquoise group: the mineral aheylite, Planerite (redefined), turquoise and coeruleolactite. Mineralogical Magazine, 62, 93–111.

Giuseppetti, G., Mazzi, F., and Tadini, C. (1989) The crystal structure of chalcosiderite, $CuFe_6^{3+}(PO)_4(OH)_8.4H_2O$. Neues Jahrbuch für Mineralogie Monatshefte, 227–239.

Hull, S., Fayek, M., Mathien, F.J., Shelley, P., and Roler Durand, K. (2008) A new approach to determining the geological provenance of turquoise artifacts using hydrogen and copper stable isotopes. Journal of Archaeological Science, 35, 1355–1369.

Johansson, U., Holmgren, A., Forsling, W., and Frost, R. (1998) Isotopic exchange of kaolinite hydroxyl protons: A diffuse reflectance infrared Fourier transform spectroscopy study. Analyst, 123, 641–645.

Madejová, J. and Komadel, P. (2001) Base line studies of the clay minerals society source clays: Infrared methods. Clays and Clay Minerals, 49, 410–432.

Patrier, P., Beaufort, D., Meunier, A., Eymery, J-P., and Petit, S. (1991) Determination of the nonequilibrium ordering state in epidote from ancient geothermal field of Saint Martin: Application of Mössbauer spectroscopy. American Mineralogist, 76, 602–610.

Prost, R., Dameme, A., Huard, E., Driard, J., and Leydecker, J.P. (1989) Infrared study of structural OH in kaolinite, dickite, nacrite, and poorly crystalline kaolinite at 5 to 600 K. Clays and Clay Minerals, 37, 464–468.

Rancourt, D.G. (1994) Mössbauer spectroscopy of minerals. I. Inadequacy of Lorentzian-line doublets in fitting spectra arising from quadrupole splitting distributions. Physics and Chemistry of Minerals, 21, 244–249.

Rancourt, D.G. and Ping, J.Y. (1991) Voigt-based methods for arbitrary-shape static hyperfine parameter distributions in Mössbauer spectroscopy. Nuclear Instruments and Methods in Physics Research, B, 58, 85–97.

Reddy, B.J., Frost, R.L., Weier, M.L., and Martens, W.N. (2006) Ultraviolet-visible, near infrared and mid infrared reflectance spectroscopy of turquoise. Journal of Near Infrared Spectroscopy, 14, 241–250.

Robinson, K., Gibbs, G.V., and Ribbe, P.H. (1971) Quadratic elongation: a quantitative measure of distortion in coordination polyhedral. Science, 172, 567–570.

Sherman, D.M. (1985) SCF-Xα-SW MO study of Fe–O and Fe–OH chemical bonds; Applications to the Mössbauer spectra and Magnetochemistry of hydroxyl-bearing Fe^{3+} oxides and silicates. Physics and Chemistry of Minerals, 12, 311–314.

Sklavounos, S., Ericsson, T., Filippidis, A., Michailidis, K., and Kougoulis, C. (1992) Chemical, X-ray and Mössbauer investigation of a turquoise from the Vathi area volcanic rocks, Macedonia, Greece. Neues Jahrbuch für Mineralogie Monatshefte, 469–480.

Van Wambeke, L. (1971) The problem of cation defiency in some phosphates due to alteration processes. American Mineralogist, 56, 1366–1384.